Understanding Spacecraft Trajectories through Detached Magnetotail Interchange Heads

Evgeny V. Panov[1], San Lu[2], Philip L. Pritchett[3]

[1]Space Research Institute, Austrian Academy of Sciences, Graz, Austria.
[2]Department of Earth, Planetary, and Space Sciences, University of California, Los Angeles, CA, USA
[3]Department of Physics and Astronomy, University of California, Los Angeles, CA, USA

Key Points:

- THEMIS crossings of detached magnetotail interchange heads are compared with PIC-simulated later-stage BICI development.
- Similar signatures of the head's leading edges and trailing tails are identified in both in situ and simulated data.
- The signatures appeared to be the result of oblique (earthward/dawnward) propagation of the detached heads.

Corresponding author: E.V. Panov, `evgeny.panov@oeaw.ac.at`

Abstract

The kinetic ballooning/interchange instability (BICI) was recently found to produce azimutally narrow interchange heads extending into the dipole region from a reversed radial gradient of B_Z in the near-Earth magnetotail. In their nonlinear evolution individual heads were predicted to detach from the reversed B_Z gradient and grow into transient earthward moving northward magnetic field intensifications (dipolarization fronts; DFs). The distinguished signatures of such fronts would be their oblique propagation and cross-tail localization due to the finite k_y structure of the BICI modes. Simultaneous conjugate observations of DFs by THEMIS probes at 11 Earth's radii (R_E) downtail and of sudden brightening and growth of individual auroral beads by the all sky imagers on the ground have been suggested to be ionospheric signature of detached magnetotail interchange heads [*Panov et al.*, 2019]. Here we compare such DFs with a simulated interchange head during later(detachment)-stage BICI head development. The comparison reveals similarly structured leading edges and trailing tails in both the observed DFs and the simulated BICI head. We further identify THEMIS trajectories through the DFs and find that the trajectories were due to oblique (earthward and dawnward) DF propagation. This analysis further supports the idea that BICI indeed releases obliquely propagating azimuthally localized dipolarization fronts in the Earth's magnetotail.

Plain Language Summary

The terrestrial magnetic field lines on the anti-sunward side of the Earth forming an elongated structure (the magnetotail) are periodically disrupted by magnetic reconnection. Which processes and at which distance from Earth onset magnetotail reconnection? An instability was recently found to produce azimutally narrow heads that intrude into the dipole region from the near-Earth magnetotail. At their later stages of development individual heads were predicted to grow into transient earthward moving northward magnetic field intensifications (dipolarization fronts; DFs), which under the right conditions may lead to a full-scale magnetotail disruption. By combining sophisticated high-performance computing plasma simulations with multi-point in situ observations by the NASA's Time History of Events and Macroscale Interactions during Substorms (THEMIS) probes, we show that under the right magnetotail conditions the dipolarization fronts are indeed generated by the instability at about ten Earth's radii downtail in the transition region between the geomagnetic dipole and tail fields.

1 Introduction

Reconnection in the tails of planetary magnetospheres is essential for global circulation of the magnetospheric magnetic flux [*Dungey*, 1961; *Vasyliunas*, 1983]. Observationally, it has been shown that magnetic flux transport in the tails is highly intermittent occurring in an explosive manner through transient northward magnetic field (B_Z) intensifications (dipolarization fronts) [*Russell et al.*, 1998; *Nakamura et al.*, 2002; *Sundberg et al.*, 2012]. At Earth such transport may constitute over two thirds of the whole magnetic flux transport into the inner magnetosphere [*Baumjohann et al.*, 1990; *Angelopoulos et al.*, 1994].

Presently, the exact mechanisms driving the magnetotail reconnection remain unresolved [*Sitnov et al.*, 2019]. Various theoretical models suggest that reconnection emerge spontaneously through tearing instability [*Sitnov et al.*, 2013] or could be externally driven through forming a thin current sheet [*Hesse and Schindler*, 2001], for instance by increasing the lobe pressure or by current sheet bending [*Kivelson and Hughes*, 1990]. Internal accelerated plasma sheet thinning has been suggested to occur due to an interchange mechanism [*Pontius and Wolf*, 1990; *Yang et al.*, 2011a; *Hu et al.*, 2011; *Bessho and Bhattacharjee*, 2014]. More recent theoretical investigations of the magnetotail configurations with a reversed radial gradient of B_Z have suggested interchange-based reconnection driving mechanisms such as the magnetohydrodynamic "B_Z-hump" instability [*Merkin and Sitnov*, 2016; *Birn et al.*, 2018] and non-linear growth of azimuthally-confined earthward-intruding depleted plasma tubes (interchange heads) in the course of the kinetic ballooning/interchange instabilitiy (BICI) development [*Pritchett and Coroniti*, 2011, 2013; *Pritchett et al.*, 2014]. When the ratio between the plasma and the magnetic field pressures in the equatorial plane (β_{eq}) was <100 the non-linear BICI evolution released azimuthally-localized interchange heads with a significant earthward propagation velocity component and the basic properties of the magnetotail dipolarization fronts [*Ohtani et al.*, 2004; *Runov et al.*, 2011]. For β_{eq} exceeding ~500, BICI has been predicted to disrupt the magnetotail globally by the reconnection in the wakes behind the heads.

Can certain dipolarization fronts produced by different mechanisms be discriminated from others? Using Particle-In-Cell (PIC) simulation run of BICI development in a charged current sheet, we show an example of an interchange head at later (head detachment) stage of BICI simulations that had a finite radial component of the propagation velocity at the beginning of its detachment from the reversed B_Z gradient. Because of azimuthal drift of the interchange heads (the drift would be dawnward for charged current sheets [*Nishimura et al.*, 2016; *Panov and Pritchett*, 2018a]), the shown BICI head propagated at about 45° to the earthward direction. We further compare the simulation results with Time History of Events and Macroscale Interactions during Substorms (THEMIS) [*Angelopoulos*, 2008] probes' observations of two dipolarization fronts on 26 February 2009 between 5:52 and 6:00 UT and on 15 February 2008 between 9:51 and 9:59 UT, which were identified earlier amidst long chains of dawnward drifting BICI heads and simultaneously with sudden brightening and growth of individual auroral beads seen in conjugate ground all sky imager observations [*Panov et al.*, 2019]. We use magnetotail observations provided by the THEMIS probes' fluxgate magnetometers (FGM) [*Auster et al.*, 2008], electrostatic analyzers' (ESA) [*McFadden et al.*, 2008] particle detectors and electric field instruments (EFI) [*Bonnell et al.*, 2008].

2 Interchange Head during Later-Stage BICI Development

Figure 1 shows the results from 3D PIC simulation of BICI using the electron (charged) current sheet. This simulation run was used earlier in *Panov and Pritchett* [2018b], where the simulation setup is explained in Appendix A. The y coordinate in all simulation panels is directed toward dawn; the x coordinate is directed tailward. Panels (a-e) show the later-stage ($\Omega_{i0}t$=244) BICI development in the equatorial plane at the beginning of detachment of one BICI head from the higher-B_Z region (x/ρ_{i0} >25). As seen in the B_Z magnetic field component (panel (a)), the detaching head has a sharp leading edge (a narrow reddish B_Z region indicated by the white text arrow in the upper left corner). The leading edge is located at the front of the earthward directed flow channel (bluish stripe in panel (b)). The flow channel is also seen as an enhanced B_Z stripe behind the leading edge, which is indicated by the 'Trailing tail' text arrow in panel (a). The tailward end of the trailing tail is almost disconnected from the high B_Z region, indicating BICI head detachment. The leading edge is aligned quasi-perpendicular to the trailing tail. Since B_Z is positive everywhere (the minimum value of B_Z in Figure 1a was $0.02B_0$), there has been no change in magnetic topology (i.e., no reconnection). Both the trailing tail and the flow channel are oriented diagonally in Figure 1. Such oblique orientation and propagation of the leading edge and the trailing tail is due to the initial dawnward drift of the head (the dawnward drift can be understood from Figure 6 below, e.g., by tracking the dawnward motion of the tailward end of the trailing tail from y/ρ_{i0}=28 at $\Omega_{i0}t$=209.3 to y/ρ_{i0}=43 at $\Omega_{i0}t$=254.69; see also [*Panov and Pritchett*, 2018a]).

Ahead of the leading edge the ions move dawnward, whereas on the dusk side of the trailing tail V_Y is directed duskward (panel (c)). There are disturbances in the sum of the ion, electron and magnetic field pressures (panel (d)) and also in the ratio of the plasma pressure to the magnetic field pressure (plasma β) (panel (e)) that are associated with the leading edge of the detaching BICI head. The plasma β is significantly lower behind the leading edge and in the trailing tail.

By making various cuts of the BICI head in Figure 1 one can directly compare the PIC simulation results with spacecraft encounters of dipolarization fronts that were observed amidst dawnward drifting BICI heads. Pairs of black lines in each panel in Figure 1 connect (x/ρ_{i0},y/ρ_{i0})=(18,64) and (x/ρ_{i0},y/ρ_{i0})=(23,30) (a,b,e,f), and (x/ρ_{i0},y/ρ_{i0})=(0,56) and (x/ρ_{i0},y/ρ_{i0})=(32,35) (c,d,e,f). They indicate two cut examples (out of many) along which the magnetic field and plasma parameters are shown in Figure 2. At both cuts the sharp leading edge and the trailing tail can be seen as local maxima in B_Z (indicated by black text arrows in Figure 2). The sharp boundary of the leading edge is also clearly recognizable in the total pressure and in the plasma β (panels (e) and (f) in Figure 2). The space between the leading edge and the trailing tail is characterized by a local minimum in B_Z and a local maximum in β.

3 Interchange Head Signatures in near-Earth Dipolarization Fronts

Figure 3 shows dipolarization front crossings by THEMIS probes P3 and P4 on 26 February 2009 between 5:52 and 6:00 UT (left) and on 15 February 2008 between 9:51 and 9:59 UT (right). The two probes were located at $X_{GSM} \approx -11$ R_E. The two dipolarization fronts occurred in the presence of multiple dawnward drifting interchange heads [*Panov et al.*, 2019]. The dawnward propagation velocity of the interchange heads observed before the dipolarization front on 26 February 2009 was about 835 km/s (about 1.5 of the thermal ion velocity). The dawnward propagation velocity of the heads observed before the dipolarization front on 15 February 2008 was about 200 km/s (about 0.3 times the ion thermal velocity). The typical azimuthal scale of a head on both dates appeared to be comparable, between 1.6 R_E and 2 R_E. The minimum variance analysis revealed the dipolarization front normal direction (0.91, -0.41, 0.01) at P3 (i.e. ≈42 degrees dawnward) and (0.58, -0.81, 0.09) at P4 (i.e., ≈54 degrees dawnward). Both normals appeared to be close to the direction highlighted by the black lines in Figure 1 (≈45 degrees dawnward).

For the purpose of quantitative comparison with the present PIC simulations we note that the lobe field and plasma density in the Earth's magnetotail at the location of THEMIS probes were about 25 nT and 0.1 cm^{-3} on 26 February 2009, and 40 nT and 0.2 cm^{-3} on 15 February 2008, yielding local Alfvén velocity 1000 km/s (26 February 2009 event) and 1600 km/s (15 February 2009 event). To convert from the dimensionless units of the simulation to a physical (dimensional) value, one must multiply by a factor of $n_0 M_i V_A^2$. Assuming the proton mass and the values for the two observation dates, this factor is 0.17 nPa for the 26 February 2009 event and 0.86 nPa for the 15 February 2008 event. Since the dimensionless values for the total pressure near the front were on the order of 0.5 - 1.0, this gives quite good agreement with the observations, with the observed total pressure being about 4 times larger for the 15 February 2008 event as compared to the 26 February event 2009.

On 26 February 2009 at 5:53:30 UT P4 observed a sharp B_Z enhancement (Figure 3c) that was embedded in a fast earthward flow (Figure 3d). The enhancement manifested leading edge of a dipolarization front in a bursty bulk flow. Around 5:54 UT the same leading edge was observed by P3 (Figures 3a,b), which was located about 1 R_E dawnward from P4. In contrast to P4, the leading edge at P3 was flatter. Both P3 and P4 observed similar second increase in B_Z after the leading edge (denoted as 'Trailing tail' in Figures 3a,c). The fast earthward flow at P4 (blue line in Figure 3d) appeared to begin with the encounter of the leading edge and ceased after the trailing tail. The azimuthal ion velocity component (V_Y; green line in Figure 3d) exhibited a gentle dawnward peak at the leading edge, then a more pronounced duskward peak between the leading edge and the trailing tail, and finally another dawnward peak after the trailing tail around 5:55:30 UT.

The considered above behaviors of B_Z, V_X and V_Y at P4 (Figures 3c,d) between 5:52 and 5:56 UT (highlighted by the dashed magenta rectangle), repeat more the behavior of the corresponding simulated parameters in Figures 1a,b,c along the simulation cut connecting $(x/\rho_{i0},y/\rho_{i0})=(18,64)$ and $(x/\rho_{i0},y/\rho_{i0})=(23,30)$ (cf. the corresponding black lines in Figure 1) and in the corresponding cuts shown in Figures 2a,b. In contrast to P4, P3 observed a weaker earthward V_X and no duskward flow in V_Y between the leading edge and the trailing tail (Figure 3a,b). This behavior is more consistent with the hypothesis that P3 crossed the dipolarization front more dawnward (i.e. in agreement with the actual position of P3 relative to P4). Both P3 and P4 exhibited sharp increases (drops) in the total pressure and in the plasma β before (after) the leading edge (Figures 3e,f). These total pressure and plasma β variations are consistent with the PIC simulation results in Figures 2e,f. Similar observations were made by the same THEMIS probes on 15 February 2008 between 9:51 and 9:59 UT (right column in Figure 3). In contrast to the dipolarization front on 26 February 2009 (left column in Figure 3), the observations in the right column were collected significantly off the equatorial plane (as evident from $B_X \approx$25nT; not shown here). Due to this off-equatorial location, the dipolarization front normal appeared to be directed mainly along the Z_{GSM} axis at both P3 and P4.

To check for consistency of the plasma convection velocity patterns during the two dipolarization fronts with the corresponding patterns of the detaching BICI head in the PIC simulations, the X and Y GSM components of the electric field and of the cross-product of the electric and magnetic fields are shown in Figure 4 (THEMIS observations) and in Figure 5 (PIC simulations). Figure 4 shows data from P3 (panels a,b,e,f) and P4 (panels c,d,g,h) for the same time intervals as in Figure 3. Figure 5 shows panels in the same area and with the same virtual spacecraft paths (black lines) as in Figure 1. Note that in the simulation the electric field is much noisier (due to larger fluctuations arising from the small number of particles) than in the observations. The ion velocities are not sensitive to these high frequency fluctuations, and thus the simulation V_i can be much smoother than simulation $E\times B/B^2$ plots. Despite noise in both observed and simulated electric fields, one can clearly identify the finite earthward E_X that is associated with both the leading edge and the trailing tail (positive peaks in Figures 3a,c,e,g and bluish color in Figure 5a). The negative (dawnward) peaks of E_Y at the leading edge at P3 (Figures 3a,e) are associated with the dawnward side of the dipolarization front in the PIC simulations (Figure 5b). Behind the leading edge both P3 and P4 observed positive (duskward) periods in E_Y. Symmetrically, the X component of the cross-product of the electric and magnetic fields reflects the behavior of the Y component of the electric field, and $(E\times B/B^2)_Y$ reflects that of E_X.

The above comparisons were made between time dependent THEMIS observations and static cuts from the BICI simulation. Below we show that the signatures of the leading edges and trailing tails from THEMIS observations are also seen in the more realistic time-dependent pictures of the simulated BICI head. For this purpose, we investigated the behavior of the magnetic field and plasma parameters as would be 'observed' by a net of virtual spacecraft before and after $\Omega_{i0}t$=244. Figure 6 shows the temporal evolution of the magnetic field B_Z component with the overplotted ion velocity field. The BICI head that detached from the high-B_Z region (x/ρ_{i0} >25) before $\Omega_{i0}t$=209.38 (left) propagated to smaller x/ρ_{i0} (earthward) and to larger y/ρ_{i0} (dawnward) as $\Omega_{i0}t$ progressed (from left to right and from top to bottom in Figure 6). Despite the leading edge and the trailing tail of the BICI head persisted during the whole considered time interval, the head has grown remarkably with a sharper leading edge and a fainter broken trailing tail toward the end of the simulation interval. The B_Z disturbance associated with the leading edge encompasses as much as half of the field of view with the largest values at the leading edge's nose. The B_Z disturbances on the two flanks of the leading edge are comparable with the B_Z disturbances associated with the trailing tail at later times (when $\Omega_{i0}t$ exceeded about 230).

There are three pairs of black star/square glyphs at different (x/ρ_{i0},y/ρ_{i0}) in Figure 6 (denoted as 'A', 'B', and 'C'). The virtual spacecraft observations at the locations indicated by these glyphs are shown in the three columns in Figure 7. The relative positions of the star/square pairs qualitatively resemble more dawnward and tailward location of THEMIS P3 (corresponds to the star glyphs in Figure 6) with respect to THEMIS P4 (corresponds to the square glyphs in Figure 6) during the dipolarization front observations from Figure 3. That is the data in each column in Figure 7 are shown in the same sequence as in the two columns of Figure 3. Column A in Figure 7 shows that the leading edge and the trailing tail were observed by the virtual spacecraft next to each other. The trailing tail was as pronounced as the leading edge. These simulation results agree with THEMIS observations in Fgiure 3. In the simulations the leading edge was observed by the virtual spacecraft at the beginning of the BICI head formation and closer to the dawnward flank; the trailing tail crossed the two virtual spacecraft due to its dawnward motion. The former fact is in agreement with two probe THEMIS observations, when the first probe that encountered the trailing tail appeared to be P4 (which was located duskward from P3). To conclude, the virtual spacecraft observations are significantly more consistent with THEMIS observations than the static cuts provided in Figure 2, because they reproduce time evolution of the detached BICI head.

Obviously in other situations spacecraft might observe BICI heads at stages of BICI head detachment that are earlier or later than shown in the left column in Figure 7. Also, spacecraft might be located at other azimuthal and radial positions with respect to detaching BICI heads. To demonstrate the signatures that BICI simulations predict for in situ observations at few other locations we include virtual spacecraft observations that were collected at square/star glyph pairs 'B' and 'C' (middle and right columns in Figure 7). The 'B' column shows observations more dawnward and thus at a later time than those in column 'A'. On the contrary, the 'C' column shows observations more duskward and thus at an earlier time than those in columns 'A' and 'B'. Whereas the leading edges in the 'B' column are significantly enhanced as compared to 'A', at earlier times ('C') the dip between the leading edges and the trailing tails has not yet been formed (the B_Z profile has a step-like shape at earlier detachment stages). Despite the above differences between 'A', 'B' and 'C', in all of them one can clearly see the earthward-to-tailward reversal of V_X just after the trailing tail of the BICI head (cf. blue curves in Figures 7b,d,h,j,n,p). This reversal occurred due to dawnward component of the BICI head drift.

As demonstrated in [*Panov and Pritchett*, 2018a; *Panov et al.*, 2019], BICI development signatures were observed for hours on 15 February 2008 and on 26 February 2009. As a consequence, during the two events there were observed a number of other dipolarization fronts with detached BICI signatures. Below we consider several of them for the purpose of discussion on various stages of development of the observed detached BICI heads. Figure 8 shows the BICI head observations by P4 and P3 on 15 February 2008 between 10:22 and 10:27 UT. *Panov and Pritchett* [2018b] showed that the head drifted dawnward at a velocity of about 200 km/s. The head's azimuthal scale was on the order of 2 R_E. The step-like shape of the B_Z profile across the head is similar to the B_Z profiles from the right column in Figure 7, suggesting that the BICI head in Figure 8 crossed THEMIS probes at an earlier stage of detachment (if any). Both P3 and P4 exhibited V_X reversal at the trailing edge of the head, also consistent with Figures 7n,p.

The next two figures show single probe observations of two detached BICI heads that occurred during the event on 15 February 2008, between 6:21 and 6:26 UT by P5 in Figure 9, and between 7:10 and 7:20 UT by P4 in Figure 10. Both head encounters exhibit signatures that are similar to those demonstrated in Figure 8: step-like shapes of B_Z and clear V_X reversals. In contrast to the example from Figure 8, BICI heads in Figures 9,10 exhibited also weak signatures of separation of the leading edges from the trailing tails (seen as separate B_Z peaks in the top panels of Figures 9,10). The emerging B_Z dip between the leading edges and the trailing tails in these two examples indicates a somewhat later stage of develpment than in Figure 8.

Figure 11 shows another example of a detached BICI head, which was observed by three THEMIS probes P3-P5 on 26 February 2009 between 6:55 and 7:05 UT. As in the previous examples, the V_X reversal was clearly observed by the three probes. All three probes observed quite coherent structure of the ion flows, and a significant peak in the total pressure at the head's leading edge also. This implies a broad and intense leading edge of the BICI head, indicating later stage of development (perhaps similar to $\Omega_{i0}t$=254.69 in Figure 6 or later). A further support of this hypothesis is provided in B_Z observations by P3 in the top panel of the middle column in Figure 11. In this panel very small values of B_Z in the head's wake (in several points B_Z appeared to be slightly negative) are consistent with the expected simulation results of the BICI head development in the high-β environment [*Pritchett and Coroniti*, 2011, 2013; *Pritchett et al.*, 2014]. Note that during this crossing P3 observed β that exceeded 10^3 in the wake of the BICI head (cf. bottom panel in the middle column of Figure 11).

Figure 12 shows our final BICI head example. This head crossed P3-P5 probes about 17 minutes earleir than the BICI head from Figure 11. Despite nearly identical configuration of the three THEMIS probes, it occurred that the most duskward probe P4 (right column in Figure 12) observed very weak earthward flow (less than 30 km/s). This can be explained by assuming that the major flow channel was always dawnward of P4, i.e. P4 peripherally observed the dusk side of the head. This assumption is actually in agreement with the observations from P5 (left column in Figure 12), which observed the fastest and longer duration earthward flow (and stagnation or very small tailward flows after V_X reversal, similarly to P3 and P4 observations in Figure 3): Taking into account that P5 was located azimuhtally midway from P4 to P3 (middle column in Figure 12), P5 occurred to have crossed the middle of the BICI head, and P3 observed the dawnward side of the head. This allows to conclude on the azimuthal size of the head: comparable to the azimuthal distance between P3 and P4 about 1 R_E.

The above examples of detaching and detached BICI heads are not the only ones during the two long-lasting BICI events, but the clearest and most interesting, showcasing variety of spacecraft trajectories and highlighting differences in observations along the trajectories and at different stages of BICI development. Note that the simulation was a prediction made before the present comparison with observations and we did not attempt to "fit" the present observations. Clearly, the simulation does not have the spatial resolution to serve as a precise model of the entire near-Earth plasma sheet region. Because of many numerical limitations we do not expect the simulation to identically repeat the observations also. One of such limitations is the size of the simulation box and various effects, e.g. at the simulation box boundaries. It may well be that the simulation box is much smaller than the possible volume of the actual magnetotail in which BICI might operate (especially in the X-direction). The latter fact might allow the observed BICI heads to propagate longer distances both radially and azimuthally before being encountered by a spacecraft. One other technical constraint is the artificial mass ratio that was used in the simulation. These two major limitations are expected to be responsible for some of the differences between the simulation and observations (e.g. sharper leading edge and larger ratio of its B_Z to the background field in Figure 3c). Despite the above limitations, the simulation appeared to reproduce a very substantial number of the features observed by THEMIS without any attempt to make a detailed fit to the data.

4 Important Details of BICI Head Development

The convection electric field in Figure 5 reveals that the leading edge and the trailing tail of the simulated interchange head move as a whole. Ahead of the leading edge there is a thin layer with tailward plasma convection due two vorticity at the sides of the interchange head. In the case of the dawnward propagating interchange head the vorticity is more prominent on the dawnward side. This picture is generally consistent with THEMIS electric field and convection velocity observations in Figure 4. The consistency between the simulated interchange head and the observed dipolarization fronts points out to BICI as the dipolarization front generation mechanism.

BICI heads were also predicted to appear and identified in THEMIS data for neutral current sheets, in which they drift in the dusk direction [*Pritchett and Coroniti*, 2010; *Panov et al.*, 2012a; *Pritchett and Coroniti*, 2013]. Different possible oblique motions of the BICI generated dipolarization fronts are expected to modify the suggested particle injection and acceleration mechanisms at dipolarization fronts that were predicted using, e.g., test particle simulations in magnetohydrodynamic models [*Yang et al.*, 2011b; *Birn et al.*, 2013; *Sorathia et al.*, 2018; *Ukhorskiy et al.*, 2018]. Note that as the global magnetohydrodynamic simulations showed, dipolarization fronts that were produced by reconnection at more tailward locations may shortly deviate from their otherwise radial propagation on their way to the dipolar field lines [*Wiltberger et al.*, 2015; *Ukhorskiy et al.*, 2018; *Merkin et al.*, 2019]. We also admit that the dipolarization fronts released by BICI may later be forced to move more radially by the ambient plasma.

The present analysis also reveals how some azimuthally narrow dipolarization fronts may be formed. We note that heterogeneity of the magnetotail current sheet might be another way to produce azimuthally narrow dipolarization fronts [e.g., *Lu et al.*, 2015; *Fujimoto*, 2016]. In contrast to the dipolarization fronts released by BICI, such scenarios would need reconnection in the first place.

According to previous studies of the events presented, BICI was hours long operating in the transition region between the dipole and tail field [*Panov and Pritchett*, 2018a; *Panov et al.*, 2019]. That is, statistically, only few out of tens of BICI heads would succeed to detach from the reversed B_Z gradient. Because reversed magnetotail B_Z gradient also appears transiently at reconnection fronts, BICI may also appear as a secondary reconnection front instability [*Pritchett*, 2015]. Such a secondary BICI instability would be possible if BICI heads had significantly smaller azimuthal scales than in the present events ($\ll$2 R_E; the BICI head azimuthal scale depends on the ratio between B_Z and the lobe field), or if BICI appeared at broader dipolarization fronts (dipolarization fronts larger than 6 R_E were recently observed in the near-Earth plasma sheet [*Panov et al.*, 2019]). Interestingly, a secondary interchange (Rayleigh-Taylor type) instability is known to occur in the exhaust of reconnection jets in the solar corona [*Innes et al.*, 2014].

5 Relevance to Magnetosphere-Ionosphere Coupling

The presented THEMIS events showcase the class of DFs that were generated by BICI. One of the main conclusions of the BICI simulations [*Pritchett and Coroniti*, 2011; *Pritchett et al.*, 2014] has been that DFs can be formed and propagate without the need for reconnection to have occurred. The BICI triggering occurs due to the reversed radial gradient of the vertical component of the magnetic field (B_Z). Such reversed B_Z gradient was indeed found shortly before dipolarization fronts in Figure 3 and 4 [*Panov et al.*, 2019]. An apt analogy of the described process of dipolarization front formation by BICI from everyday life would be water dripping from a roof edge when it rains: water drops stretch downward before detaching (reconnecting) and falling from the edge. Indeed, in the PIC results shown in Figure 1, the B_Z field is still positive everywhere, indicating that there has been no change in magnetic topology and hence strictly speaking no onset of reconnection. Similarly, more global earthward propagating dipolarization front is predicted to appear before reconnection in both magnetohydrodynamic [*Merkin and Sitnov*, 2016; *Birn et al.*, 2018] and kinetic [*Pritchett*, 2015; *Sitnov et al.*, 2017] simulations of the "B_Z-hump" instability. This sequence of events would be phenomenologically similar to the so-called 'inside-out' substorm scenario [*Lui*, 1996], when first an instability (such as ballooning/interchange or the B_Z-hump instability) is needed to appear in the magnetotail. Thus the revealed class of DFs is different from those appeared as a consequence of reconnection [e.g. *Angelopoulos et al.*, 2013].

This new class of DFs appears to drive specific consequences for the magnetosphere-ionosphere coupling. During the two presented DFs there occurred ionospheric pseudo-breakups with local current systems and auroral bright spots originating from azimuthal beads/rays [*Panov et al.*, 2019]. Other dipolarization fronts amidst azimuthally drifting interchange heads [*Uritsky et al.*, 2009; *Sergeev et al.*, 2009; *Panov et al.*, 2012b] were found to be related to a full scale substorm onset [*Panov et al.*, 2012a]. During all these reported events at least one of THEMIS probes occasionally crossed the neutral sheet ($B_X \approx 0$) during BICI activity. This allowed to estimate β_{eq} during the events. It appeared that in the events that ended with localized ionospheric pseudo-breakups β_{eq} did not exceed few tens [*Panov et al.*, 2019], while during full scale substorm events [*Panov et al.*, 2012a] β_{eq} was few hundreds (with the peak values exceeding 2000; not shown here), consistent with BICI simulation predictions. Note that during the full scale substorm event on 28 February 2008, THEMIS P2 and P3 observed direct signatures of reconnection such as oppositely directed plasma flows and negative B_Z [*Panov et al.*, 2012b] (cf. Figure 3). Similar relation of plasma sheet β to pseudo-breakups and substorms was recently found for a single event study of the near-Earth magnetotail conditions during fast ion flows that originated from $X_{GSM} < -21$ R_E [*Miyashita et al.*, 2018]. That is, despite differences in the dipolarization front formation and substorm scenarios between the near-Earh BICI mechanism and more tailward reconnection events [*Nagai et al.*, 2005; *Petrukovich et al.*, 2009; *Angelopoulos et al.*, 2008], the requirement of higher β_{eq} may well be common for all substorm models.

Interestingly, internal plasma sheet thinning mechanisms (magnetohydrodynamic [*Hau et al.*, 1989; *Hau*, 1991; *Hsieh and Otto*, 2015] or kinetic [*Pritchett and Coroniti*, 1994, 1995]) may also be possible in the magnetospheres of other planets. For instance, centrifugal interchange instabilities in magnetodiscs of giant planets would lead to ballooning type modes [*Kivelson and Southwood*, 2005; *Mauk et al.*, 2009]. Growth of interchange finger-like structures in magnetodiscs of giant planets may provoke reconnection following the scenario suggested for the interaction between closely located flux tubes with different entropy ('bubble-blob pairs') [*Yang et al.*, 2011a; *Hu et al.*, 2011]. It is thus may be important to take into account the present THEMIS observations and PIC simulations in various models of global circulation of the magnetospheric magnetic flux at other planets.

6 Conclusions

We compared THEMIS observations of two dipolarization fronts amidst identified earlier dawnward drifting BICI heads at $X_{GSM} \approx -11R_E$, whose appearance coincided with sudden brightening and growth of individual auroral beads, and the PIC simulations of a dawnward drifting BICI head at later stage. The revealed THEMIS trajectories through the DFs evidence oblique (earthward and dawnward) DF propagation, whose leading edges and trailing tails appeared to be structured similarly to those of the simulated interchange head. These consistencies not only further support the idea that BICI was indeed responsible for the formation of the observed DFs in the transition region between the geomagnetic dipole and tail fields, but also allows to judge on the stage of development of BICI heads at the moment of their crossing by spacecraft.

Acknowledgments
We acknowledge NASA contract NAS5-02099 for use of data from the THEMIS Mission, and specifically, for the use of FGM data supported through the German Ministry for Economy and Technology and the German Center for Aviation and Space (DLR) under

contract 50 OC 0302. The PIC simulations were performed using the High-End Computing facilities of the NASA Advanced Supercomputing Division at the Ames Research Center. The work of E.V.P. was supported by the Austrian Science Fund (FWF): I 3506-N27. E.V.P. and P.L.P. are thankful to the International Space Science Institute Bern, Switzerland for the hospitality and support and the fruitful discussions with members of the ISSI working group on "Explosive Processes in the Magnetotail". The authors are grateful to V. Angelopoulos, W. Baumjohann, R. Lysak, R. Nakamura, M.I. Sitnov, F. Toffoletto and R.A. Wolf for insightful discussions. THEMIS data are available from the Space Physics Data Facility of the Goddard Space Flight Center (http://cdaweb.gsfc.nasa.gov/). The original simulation data used to plot Figures 1, 2, 5, 6, 7, and the Supporting Information Figures F1, F2 can be downloaded from https://doi.org/10.6084/m9.figshare.12055497.

References

Angelopoulos, V. (2008), The THEMIS Mission, *Space Sci. Rev.*, *141*, 5–34, doi: 10.1007/s11214-008-9336-1.

Angelopoulos, V., C. F. Kennel, F. V. Coroniti, R. Pellat, M. G. Kivelson, R. J. Walker, C. T. Russell, W. Baumjohann, W. C. Feldman, and J. T. Gosling (1994), Statistical characteristics of bursty bulk flow events, *Journal of Geophysical Research: Space Physics*, *99*, 21, doi:10.1029/94JA01263.

Angelopoulos, V., J. P. McFadden, D. Larson, C. W. Carlson, S. B. Mende, H. Frey, T. Phan, D. G. Sibeck, K.-H. Glassmeier, U. Auster, E. Donovan, I. R. Mann, I. J. Rae, C. T. Russell, A. Runov, X.-Z. Zhou, and L. Kepko (2008), Tail Reconnection Triggering Substorm Onset, *Science*, *321*, 931, doi:10.1126/science.1160495.

Angelopoulos, V., A. Runov, X.-Z. Zhou, D. L. Turner, S. A. Kiehas, S.-S. Li, and I. Shinohara (2013), Electromagnetic energy conversion at reconnection fronts, *Science*, *341*(6153), 1478–1482, doi:10.1126/science.1236992.

Auster, H. U., K. H. Glassmeier, W. Magnes, O. Aydogar, W. Baumjohann, D. Constantinescu, D. Fischer, K. H. Fornacon, E. Georgescu, P. Harvey, O. Hillenmaier, R. Kroth, M. Ludlam, Y. Narita, R. Nakamura, K. Okrafka, F. Plaschke, I. Richter, H. Schwarzl, B. Stoll, A. Valavanoglou, and M. Wiedemann (2008), The THEMIS Fluxgate Magnetometer, *Space Sci. Rev.*, *141*, 235–264, doi:10.1007/s11214-008-9365-9.

Baumjohann, W., G. Paschmann, and H. Luehr (1990), Characteristics of high-speed ion flows in the plasma sheet, *Journal of Geophysical Research: Space Physics*, *95*, 3801–3809, doi:10.1029/JA095iA04p03801.

Bessho, N., and A. Bhattacharjee (2014), Instability of the current sheet in the earth's magnetotail with normal magnetic field, *Physics of Plasmas*, *21*(10), 102,905, doi: 10.1063/1.4899043.

Birn, J., M. Hesse, R. Nakamura, and S. Zaharia (2013), Particle acceleration in dipolarization events, *Journal of Geophysical Research (Space Physics)*, *118*, 1960–1971, doi: 10.1002/jgra.50132.

Birn, J., V. G. Merkin, M. I. Sitnov, and A. Otto (2018), MHD Stability of Magnetotail Configurations With a Bz Hump, *Journal of Geophysical Research: Space Physics*, *123*(5), 3477–3492, doi:10.1029/2018JA025290.

Bonnell, J. W., F. S. Mozer, G. T. Delory, A. J. Hull, R. E. Ergun, C. M. Cully, V. Angelopoulos, and P. R. Harvey (2008), The Electric Field Instrument (EFI) for THEMIS, *Space Sci. Rev.*, *141*, 303–341, doi:10.1007/s11214-008-9469-2.

Dungey, J. W. (1961), Interplanetary magnetic field and the auroral zones, *Physical Review Letters*, *6*(2), 47.

Fujimoto, K. (2016), Three-dimensional outflow jets generated in collisionless magnetic reconnection, *Geophysical Research Letters*, *43*, 10,557–10,564, doi: 10.1002/2016GL070810.

Hau, L.-N. (1991), Effects of steady state adiabatic convection on the configuration of the near-earth plasma sheet. II, *J. Geophys. Res.*, *96*, 5591–5596, doi:10.1029/90JA02619.

Hau, L.-N., R. A. Wolf, G.-H. Voigt, and C. C. Wu (1989), Steady state magnetic field configurations for the earth's magnetotail, *J. Geophys. Res.*, *94*, 1303–1316, doi: 10.1029/JA094iA02p01303.

Hesse, M., and K. Schindler (2001), The onset of magnetic reconnection in the magnetotail, *Earth, Planets, and Space*, *53*, 645–653, doi:10.1186/BF03353284.

Hsieh, M.-S., and A. Otto (2015), Thin current sheet formation in response to the loading and the depletion of magnetic flux during the substorm growth phase, *J. Geophys. Res.*, *120*, 4264–4278, doi:10.1002/2014JA020925.

Hu, B., R. A. Wolf, F. R. Toffoletto, J. Yang, and J. Raeder (2011), Consequences of violation of frozen-in-flux: Evidence from OpenGGCM simulations, *Journal of Geophysical Research (Space Physics)*, *116*(A6), A06223, doi:10.1029/2011JA016667.

Innes, D. E., L.-J. Guo, A. Bhattacharjee, Y.-M. Huang, and D. Schmit (2014), OBSERVATIONS OF SUPRA-ARCADE FANS: INSTABILITIES AT THE HEAD OF RECONNECTION JETS, *The Astrophysical Journal*, *796*(1), 27, doi:10.1088/0004-637x/796/1/27.

Kivelson, M. G., and W. J. Hughes (1990), On the threshold for triggering substorms, *Planet. Space Sci.*, *38*, 211–220, doi:10.1016/0032-0633(90)90085-5.

Kivelson, M. G., and D. J. Southwood (2005), Dynamical consequences of two modes of centrifugal instability in jupiter's outer magnetosphere, *Journal of Geophysical Research: Space Physics (1978–2012)*, *110*(A12), doi:10.1029/2005JA011176.

Lu, S., Q. Lu, Y. Lin, X. Wang, Y. Ge, R. Wang, M. Zhou, H. Fu, C. Huang, M. Wu, and S. Wang (2015), Dipolarization fronts as earthward propagating flux ropes: A three-dimensional global hybrid simulation, *Journal of Geophysical Research: Space Physics*, *120*, 6286–6300, doi:10.1002/2015JA021213.

Lui, A. T. Y. (1996), Current disruption in the Earth's magnetosphere: Observations and models, *Journal of Geophysical Research: Space Physics*, *101*, 13,067–13,088, doi: 10.1029/96JA00079.

Mauk, B. H., D. C. Hamilton, T. W. Hill, G. B. Hospodarsky, R. E. Johnson, C. Paranicas, E. Roussos, C. T. Russell, D. E. Shemansky, and J. Sittler, E. C. (2009), *Fundamental Plasma Processes in Saturn's Magnetosphere*, p. 281, doi:10.1007/978-1-4020-9217-6_11.

McFadden, J. P., C. W. Carlson, D. Larson, M. Ludlam, R. Abiad, B. Elliott, P. Turin, M. Marckwordt, and V. Angelopoulos (2008), The THEMIS ESA Plasma Instrument and In-flight Calibration, *Space Sci. Rev.*, *141*, 277–302, doi:10.1007/s11214-008-9440-2.

Merkin, V. G., and M. I. Sitnov (2016), Stability of magnetotail equilibria with a tailward B_z gradient, *J. Geophys. Res.*, *121*, 9411–9426, doi:10.1002/2016JA023005.

Merkin, V. G., E. V. Panov, K. A. Sorathia, and A. Y. Ukhorskiy (2019), Contribution of bursty bulk flows to the global dipolarization of the magnetotail during an isolated substorm, *Journal of Geophysical Research: Space Physics*, *124*(11), 8647–8668, doi: 10.1029/2019JA026872.

Miyashita, Y., V. Angelopoulos, K. Fukui, and S. Machida (2018), A Case Study of Near-Earth Magnetotail Conditions at Substorm and Pseudosubstorm Onsets, *Geophys. Res. Lett.*, *45*, 6353–6361, doi:10.1029/2018GL078589.

Nagai, T., M. Fujimoto, R. Nakamura, W. Baumjohann, A. Ieda, I. Shinohara, S. Machida, Y. Saito, and T. Mukai (2005), Solar wind control of the radial distance of the magnetic reconnection site in the magnetotail, *Journal of Geophysical Research: Space Physics*, *110*(A9), doi:10.1029/2005JA011207.

Nakamura, R., W. Baumjohann, B. Klecker, Y. Bogdanova, A. Balogh, H. Rème, J. M. Bosqued, I. Dandouras, J. A. Sauvaud, K.-H. Glassmeier, L. Kistler, C. Mouikis, T. L. Zhang, H. Eichelberger, and A. Runov (2002), Motion of the dipolarization front during a flow burst event observed by Cluster, *Geophys. Res. Lett.*, *29*, 1942, doi: 10.1029/2002GL015763.

Nishimura, Y., J. Yang, P. L. Pritchett, F. V. Coroniti, E. F. Donovan, L. R. Lyons, R. A. Wolf, V. Angelopoulos, and S. B. Mende (2016), Statistical properties of substorm auroral onset beads/rays, *J. Geophys. Res.*, *121*, 8661–8676, doi:10.1002/2016JA022801.

Ohtani, S.-I., M. A. Shay, and T. Mukai (2004), Temporal structure of the fast convective flow in the plasma sheet: Comparison between observations and two-fluid simulations, *Journal of Geophysical Research (Space Physics)*, *109*, A03210, doi: 10.1029/2003JA010002.

Panov, E. V., and P. L. Pritchett (2018a), Dawnward Drifting Interchange Heads in the Earth's Magnetotail, *Geophysical Research Letters*, *45*(17), 8834–8843, doi: 10.1029/2018GL078482.

Panov, E. V., and P. L. Pritchett (2018b), Ion Cyclotron Waves Rippling Ballooning/InterChange Instability Heads, *Journal of Geophysical Research: Space Physics*, *123*(10), 8261–8274, doi:10.1029/2018JA025603.

Panov, E. V., V. A. Sergeev, P. L. Pritchett, F. V. Coroniti, R. Nakamura, W. Baumjohann, V. Angelopoulos, H. U. Auster, and J. P. McFadden (2012a), Observations of kinetic ballooning/interchange instability signatures in the magnetotail, *Geophys. Res. Lett.*, *39*, L08110, doi:10.1029/2012GL051668.

Panov, E. V., R. Nakamura, W. Baumjohann, M. Kubyshkina, A. Artemyev, V. A. Sergeev, A. A. Petrukovich, V. Angelopoulos, K. Glassmeier, J. P. McFadden, and D. Larson (2012b), Kinetic ballooning/interchange instability in a bent plasma sheet, *J. Geophys. Res.*, *117*, A06228, doi:10.1029/2011JA017496.

Panov, E. V., W. Baumjohann, R. Nakamura, P. L. Pritchett, J. M. Weygand, and M. Kubyshkina (2019), Ionospheric Footprints of Detached Magnetotail Interchange Heads, *Geophysical Research Letters*, *46*, 7237–7247, doi:10.1029/2019GL083070.

Panov, E. V., W. Baumjohann, R. Nakamura, J. M. Weygand, B. L. Giles, C. T. Russell, G. Reeves, and M. V. Kubyshkina (2019), Continent-Wide R1/R2 Current System and Ohmic Losses by Broad Dipolarization-Injection Fronts, *Journal of Geophysical Research: Space Physics*, doi:10.1029/2019JA026521.

Petrukovich, A. A., W. Baumjohann, R. Nakamura, and H. RèMe (2009), Tailward and earthward flow onsets observed by Cluster in a thin current sheet, *Journal of Geophysical Research (Space Physics)*, *114*, A09203, doi:10.1029/2009JA014064.

Pontius, J., D. H., and R. A. Wolf (1990), Transient flux tubes in the terrestrial magnetosphere, *Geophysical Research Letters*, *17*(1), 49–52, doi:10.1029/GL017i001p00049.

Pritchett, P. L. (2015), Structure of exhaust jets produced by magnetic reconnection localized in the out-of-plane direction, *Journal of Geophysical Research (Space Physics)*, *120*, 592–608, doi:10.1002/2014JA020795.

Pritchett, P. L. (2015), Instability of current sheets with a localized accumulation of magnetic flux, *Physics of Plasmas*, *22*(6), 062,102, doi:10.1063/1.4921666.

Pritchett, P. L., and F. V. Coroniti (1994), Convection and the formation of thin current sheets in the near-Earth plasma sheet, *Geophys. Res. Lett.*, *21*, 1587–1590, doi: 10.1029/94GL01364.

Pritchett, P. L., and F. V. Coroniti (1995), Formation of thin current sheets during plasma sheet convection, *J. Geophys. Res.*, *100*, 23,551–23,566, doi:10.1029/95JA02540.

Pritchett, P. L., and F. V. Coroniti (2010), A kinetic ballooning/interchange instability in the magnetotail, *J. Geophys. Res.*, *115*, A06301, doi:10.1029/2009JA014752.

Pritchett, P. L., and F. V. Coroniti (2011), Plasma sheet disruption by interchange-generated flow intrusions, *Geophys. Res. Lett.*, *38*, L10102, doi:10.1029/2011GL047527.

Pritchett, P. L., and F. V. Coroniti (2013), Structure and consequences of the kinetic ballooning/interchange instability in the magnetotail, *J. Geophys. Res.*, *118*, 146–159, doi: 10.1029/2012JA018143.

Pritchett, P. L., F. V. Coroniti, and Y. Nishimura (2014), The kinetic ballooning/interchange instability as a source of dipolarization fronts and auroral streamers, *J. Geophys. Res.*, *119*, 4723–4739, doi:10.1002/2014JA019890.

Runov, A., V. Angelopoulos, X.-Z. Zhou, X.-J. Zhang, S. Li, F. Plaschke, and J. Bonnell (2011), A THEMIS multicase study of dipolarization fronts in the magnetotail plasma sheet, *Journal of Geophysical Research (Space Physics)*, *116*, A05216, doi: 10.1029/2010JA016316.

Russell, C. T., K. K. Khurana, D. E. Huddleston, and M. G. Kivelson (1998), Localized Reconnection in the Near Jovian Magnetotail, *Science*, *280*, 1061, doi: 10.1126/science.280.5366.1061.

Sergeev, V., V. Angelopoulos, S. Apatenkov, J. Bonnell, R. Ergun, R. Nakamura, J. McFadden, D. Larson, and A. Runov (2009), Kinetic structure of the sharp injection/dipolarization front in the flow-braking region, *Geophys. Res. Lett.*, *36*(21), L21105, doi:10.1029/2009GL040658.

Sitnov, M. I., N. Buzulukova, M. Swisdak, V. G. Merkin, and T. E. Moore (2013), Spontaneous formation of dipolarization fronts and reconnection onset in the magnetotail, *Geophysical Research Letters*, *40*, 22–27, doi:10.1029/2012GL054701.

Sitnov, M. I., V. G. Merkin, P. L. Pritchett, and M. Swisdak (2017), Distinctive features of internally driven magnetotail reconnection, *Geophysical Research Letters*, *44*(7), 3028–3037.

Sitnov, M. I., J. Birn, B. Ferdousi, E. Gordeev, Y. Khotyaintsev, V. G. Merkin, T. Motoba, A. Otto, E. V. Panov, P. L. Pritchett, F. Pucci, J. Raeder, A. Runov, V. A. Sergeev, M. Velli, and X. Z. Zhou (2019), Explosive magnetotail activity, *Space Sci. Rev.*, p. 215:31, doi:https://doi.org/10.1007/s11214-019-0599-5.

Sorathia, K. A., A. Y. Ukhorskiy, V. G. Merkin, J. F. Fennell, and S. G. Claudepierre (2018), Modeling the depletion and recovery of the outer radiation belt during a geomagnetic storm: Combined mhd and test particle simulations, *Journal of Geophysical Research: Space Physics*, *123*(7), 5590–5609.

Sundberg, T., J. A. Slavin, S. A. Boardsen, B. J. Anderson, H. Korth, G. C. Ho, D. Schriver, V. M. Uritsky, T. H. Zurbuchen, J. M. Raines, D. N. Baker, S. M. Krimigis, R. L. McNutt, Jr., and S. C. Solomon (2012), MESSENGER observations of dipolarization events in Mercury's magnetotail, *Journal of Geophysical Research (Space Physics)*, *117*, A00M03, doi:10.1029/2012JA017756.

Ukhorskiy, A. Y., K. A. Sorathia, V. G. Merkin, M. I. Sitnov, D. G. Mitchell, and M. Gkioulidou (2018), Ion Trapping and Acceleration at Dipolarization Fronts: High-Resolution MHD and Test-Particle Simulations, *Journal of Geophysical Research (Space Physics)*, *123*, 5580–5589, doi:10.1029/2018JA025370.

Uritsky, V. M., J. Liang, E. Donovan, E. Spanswick, D. Knudsen, W. Liu, J. Bonnell, and K. H. Glassmeier (2009), Longitudinally propagating arc wave in the pre-onset optical aurora, *Geophys. Res. Lett.*, *36*, L21103, doi:10.1029/2009GL040777.

Vasyliunas, V. M. (1983), Plasma distribution and flow, Physics of the Jovian Magnetosphere, edited by Dessler, A. J., pp. 395–453.

Wiltberger, M., V. Merkin, J. G. Lyon, and S. Ohtani (2015), High-resolution global magnetohydrodynamic simulation of bursty bulk flows, *Journal of Geophysical Research: Space Physics*, *120*, 4555–4566, doi:10.1002/2015JA021080.

Yang, J., R. A. Wolf, and F. R. Toffoletto (2011a), Accelerated thinning of the near-Earth plasma sheet caused by a bubble-blob pair, *Geophysical Researcg Letters*, *38*(1), L01107, doi:10.1029/2010GL045993.

Yang, J., F. R. Toffoletto, R. A. Wolf, and S. Sazykin (2011b), RCM-E simulation of ion acceleration during an idealized plasma sheet bubble injection, *Journal of Geophysical Research (Space Physics)*, *116*, A05207, doi:10.1029/2010JA016346.

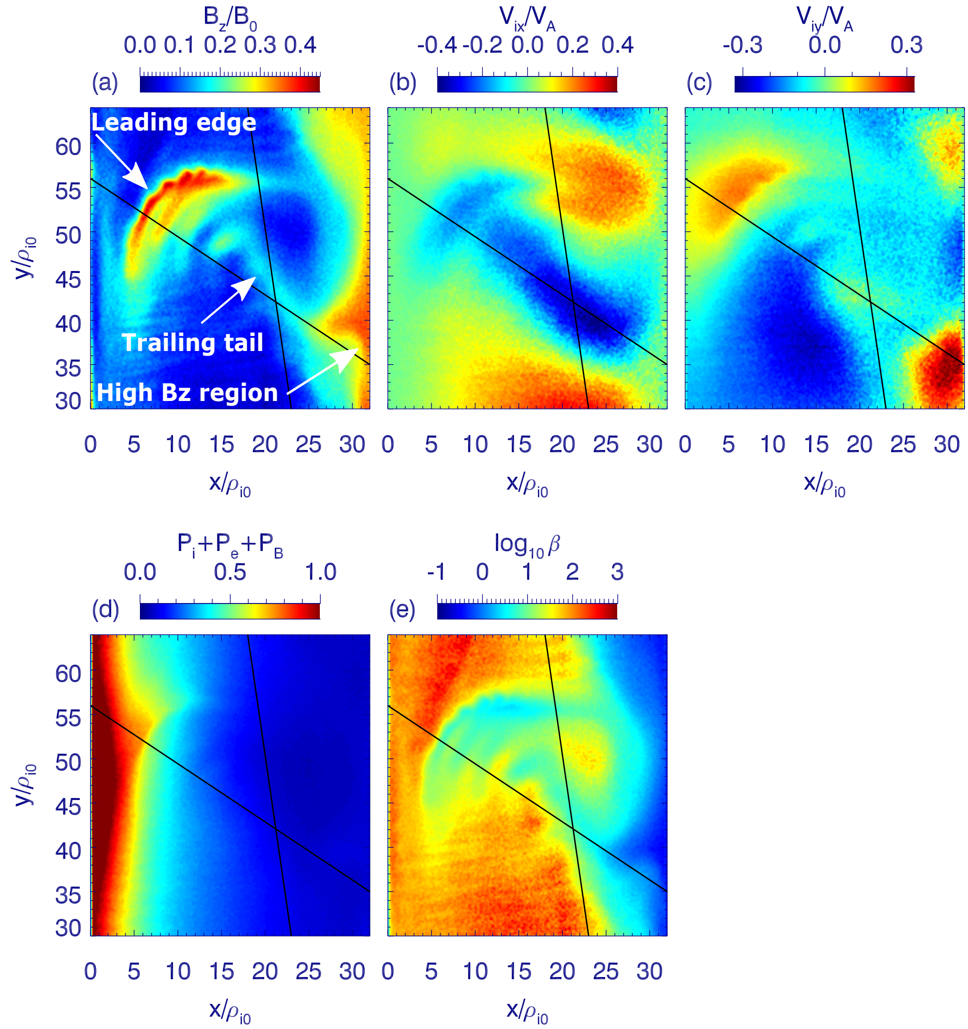

Figure 1. Results from 3D PIC simulation of BICI development in the electron (charged) current sheet at $\Omega_{i0}t$=244 as seen in the B_Z magnetic field component (a), in the V_X (b) and V_Y (c) ion velocity components, in the sum of the ion, electron and magnetic field pressures (d), and in the ratio of the plasma pressure to the magnetic field pressure (plasma β) (e).

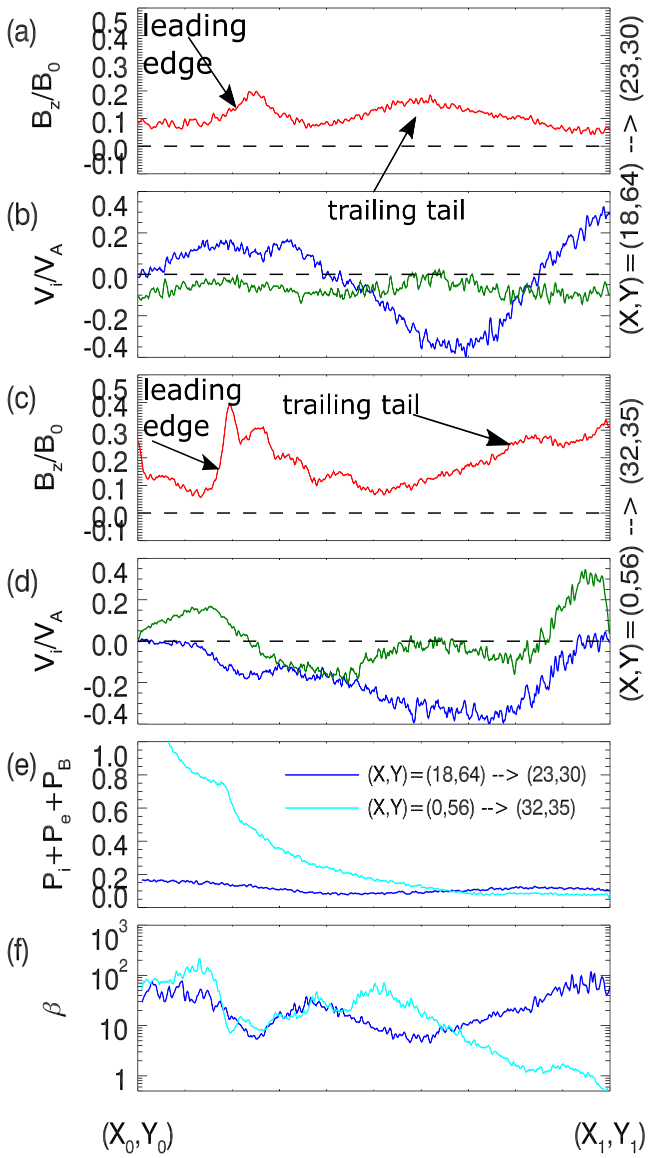

Figure 2. 1D cuts of the plots from Figure 1 between $(x/\rho_{i0},y/\rho_{i0})=(18,64)$ and $(x/\rho_{i0},y/\rho_{i0})=(23,30)$ (a,b,e,f), and between $(x/\rho_{i0},y/\rho_{i0})=(0,56)$ and $(x/\rho_{i0},y/\rho_{i0})=(32,35)$ (c,d,e,f) for B_Z (a,c), V_X (blue) and V_Y (green) (b,d), the sum of the ion, electron and magnetic field pressures (e) and the ratio of the plasma pressure to the magnetic field pressure (plasma β) (f).

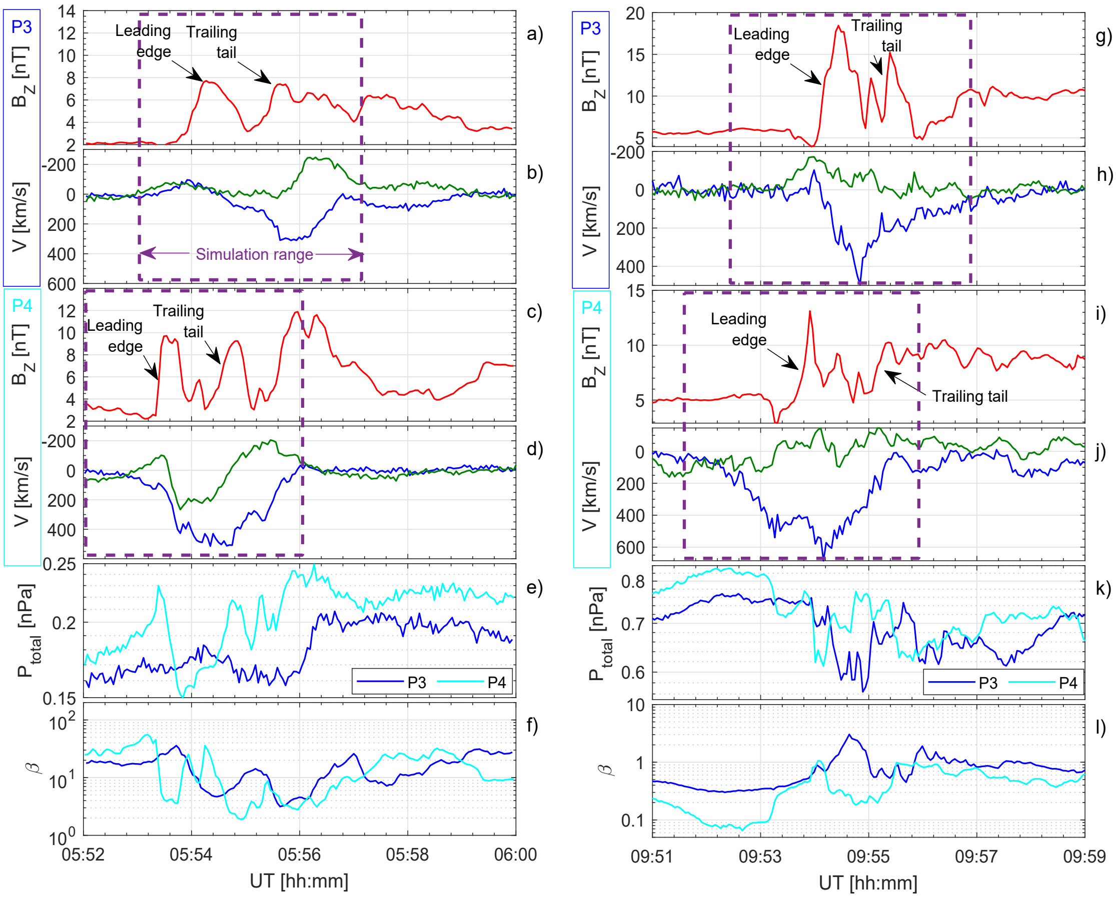

Figure 3. (left) THEMIS P3 (a,b,e,f) and P4 (c,d,e,f) observations during dipolarization front crossing on 26 February 2009 between 5:52 and 6:00 UT: GSM B_Z magnetic field component (a,c), GSM V_X (blue) and V_Y (green) ion velocity components (b,d) (note that the ordinates are reversed in the ion velocity panels (facing downward)), the sum of the ion, electron and magnetic field pressures (e) and the ratio of the plasma pressure to the magnetic field pressure (plasma β). (right) Same as left for dipolarization front observations on 15 February 2008 between 9:51 and 9:59 UT.

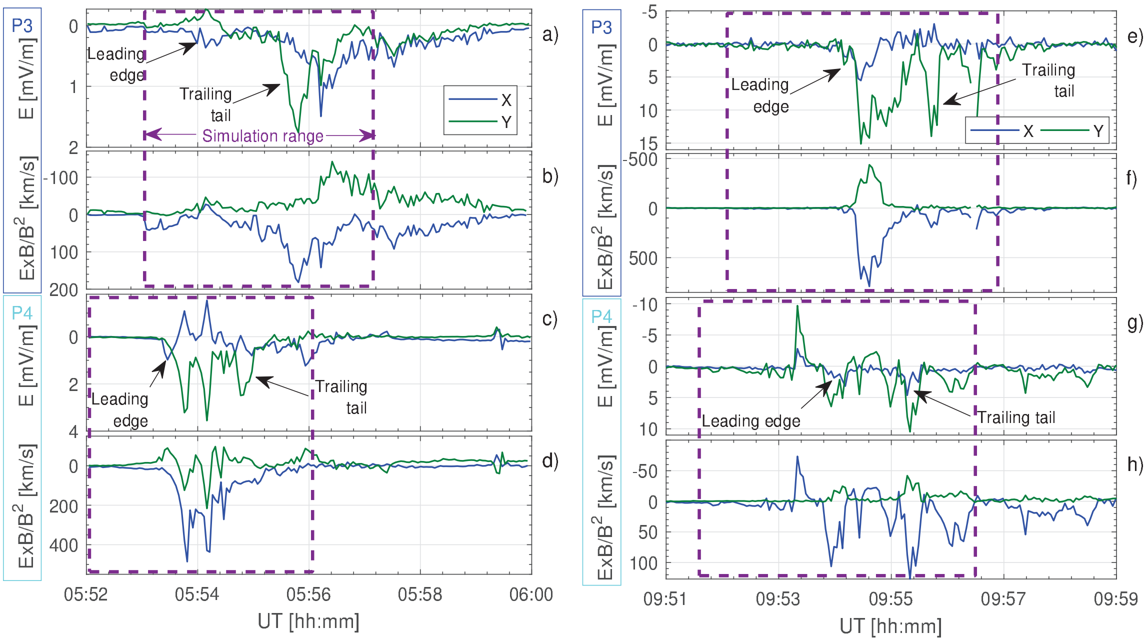

Figure 4. X and Y GSM components of the electric field (a,c,e,g) and of the cross-product of the electric and magnetic fields (b,d,f,h) from P3 (a,b,e,f) and P4 (c,d,g,h) for the same time intervals as in Figure 3. Note that the ordinates are reversed such that they are facing downward.

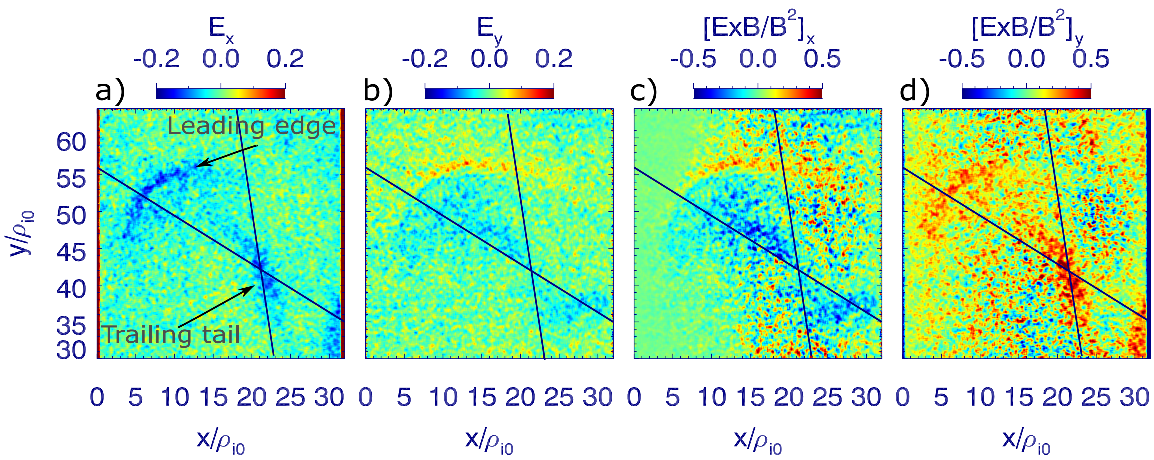

Figure 5. Results from the same 3D PIC simulation and in the same area as in Figure 1 as seen in E_X (a), in E_Y (b), in $(E\times B/B^2)_X$ (c) and in $(E\times B/B^2)_Y$ (d).

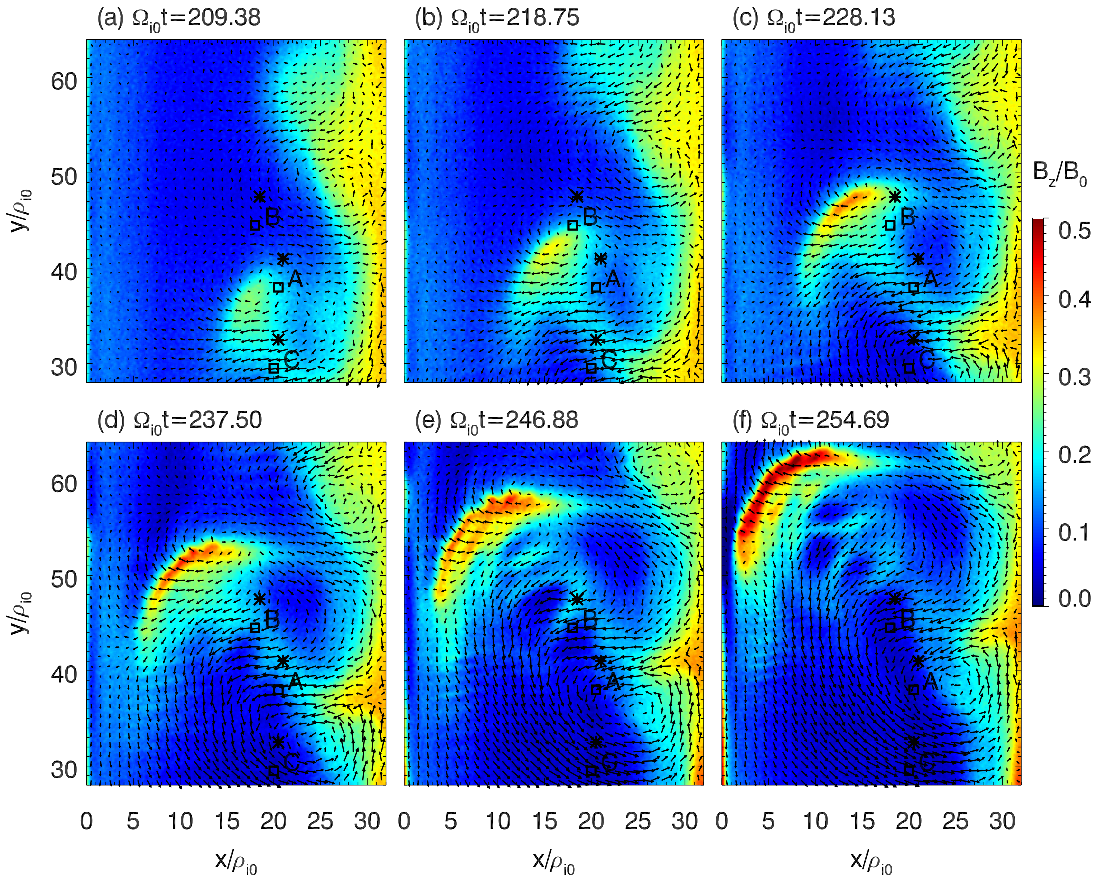

Figure 6. Results from 3D PIC simulation of BICI development in the electron (charged) current sheet as seen in the B_Z magnetic field component at six equidistant time instants between $\Omega_{i0}t$=209.38 and $\Omega_{i0}t$=254.69. The ion velocity field is overplotted by black arrows. There are three pairs of black star/square glyphs at different (x/ρ_{i0},y/ρ_{i0}): at (21,41) and (20.5,38) denoted as 'A', at (18.5,47.5) and (18,44.5) denoted as 'B', and at (20.5,32.5) and (20,29.5) denoted as 'C'. These glyphs indicate locations of pairs of the virtual spacecraft whose 'observations' are shown in Figure 7. See Supporting Information video S1 and figures F1 and F2 for snapshots of B_Z, total pressure and plasma β at other times of the simulation.

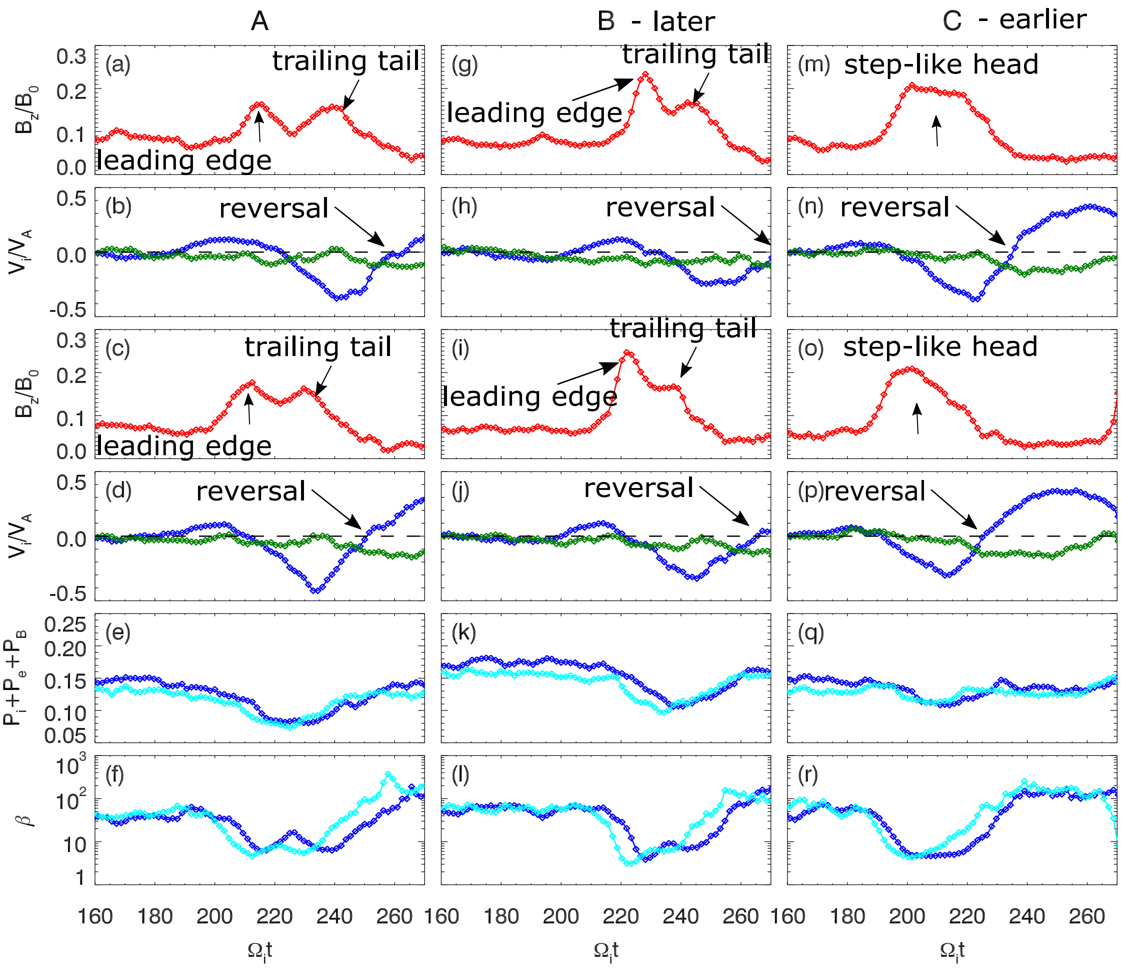

Figure 7. Each column in the figure shows virtual spacecraft observations at the locations that are marked up by the black star/square glyph pairs in Figure 6: cf. left column for pair 'A', middle for 'B' and right for 'C'. Each column has the same layout as in Figure 2.

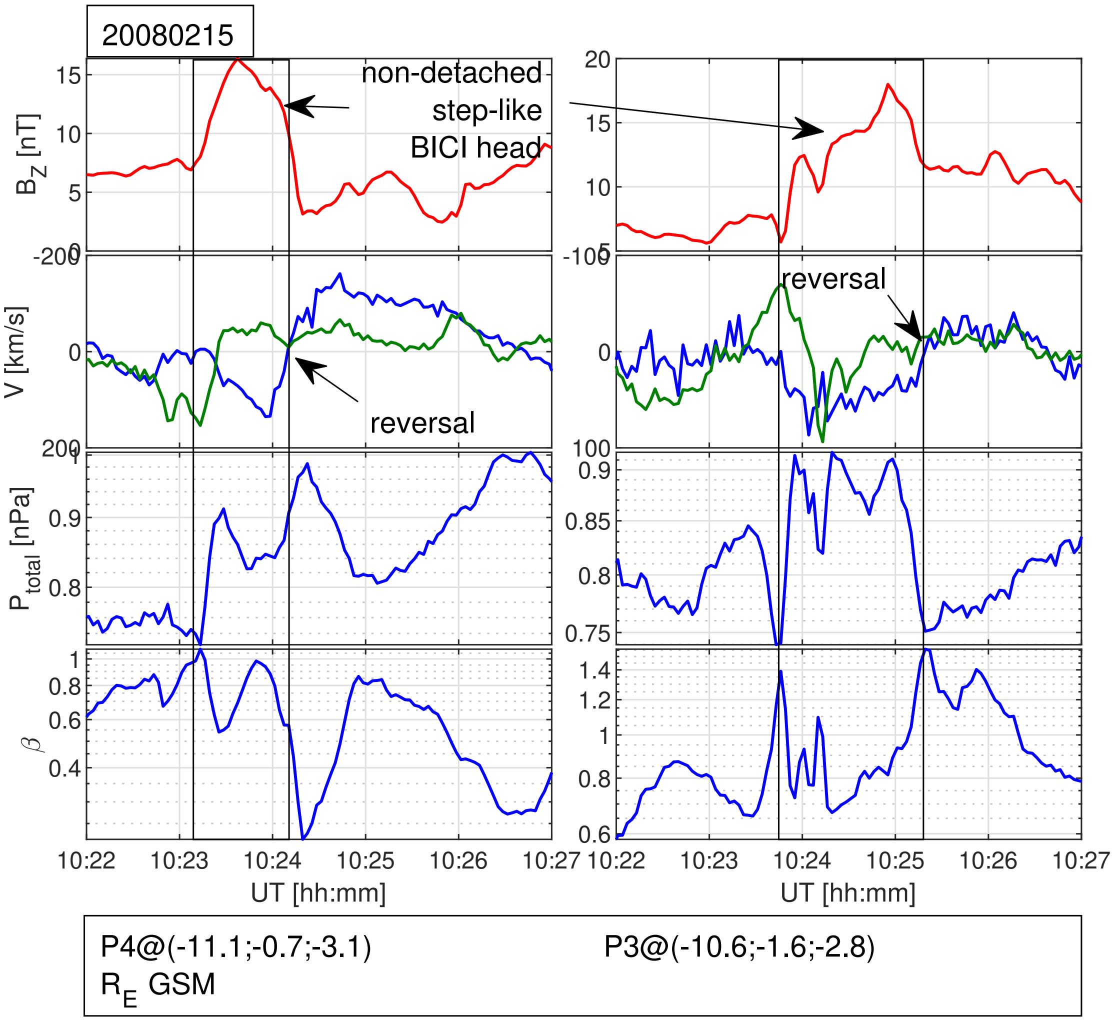

Figure 8. THEMIS P4 (left) and P3 (right) observations during dipolarization front crossing on 15 February 2008 between 10:22 and 10:27 UT: (from top to bottom) GSM B_Z magnetic field component, GSM V_X (blue) and V_Y (green) ion velocity components, the sum of the ion, electron and magnetic field pressures, and the ratio of the plasma pressure to the magnetic field pressure (plasma β). GSM THEMIS location corresponding to the middle of the time interval is provided at the bottom of each column.

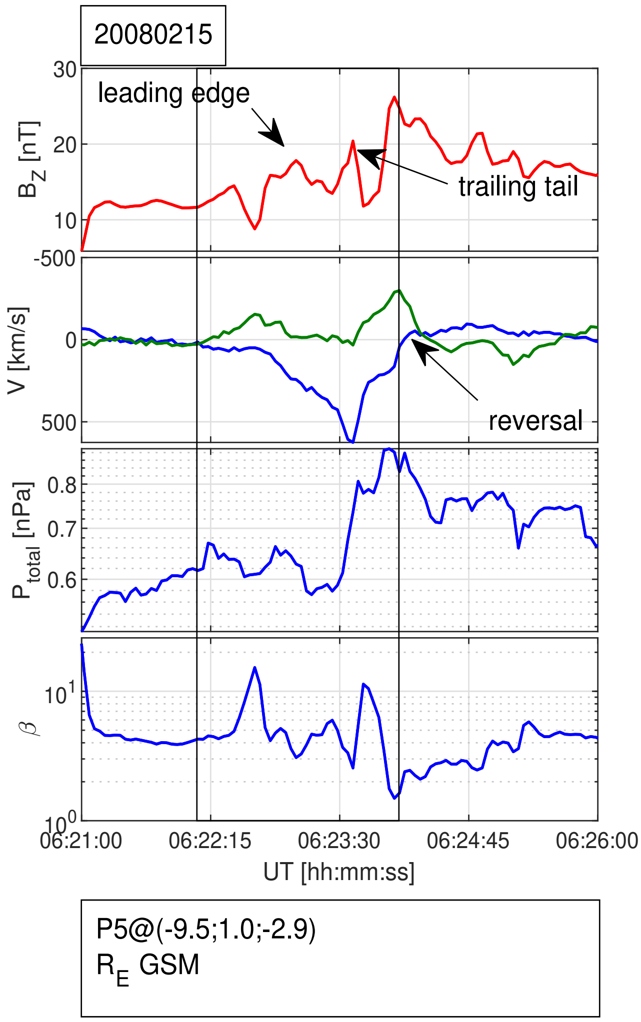

Figure 9. THEMIS P5 observations during dipolarization front crossing on 15 February 2008 between 6:21 and 6:26 UT. The data are presented in the same layout as each column in Figure 8.

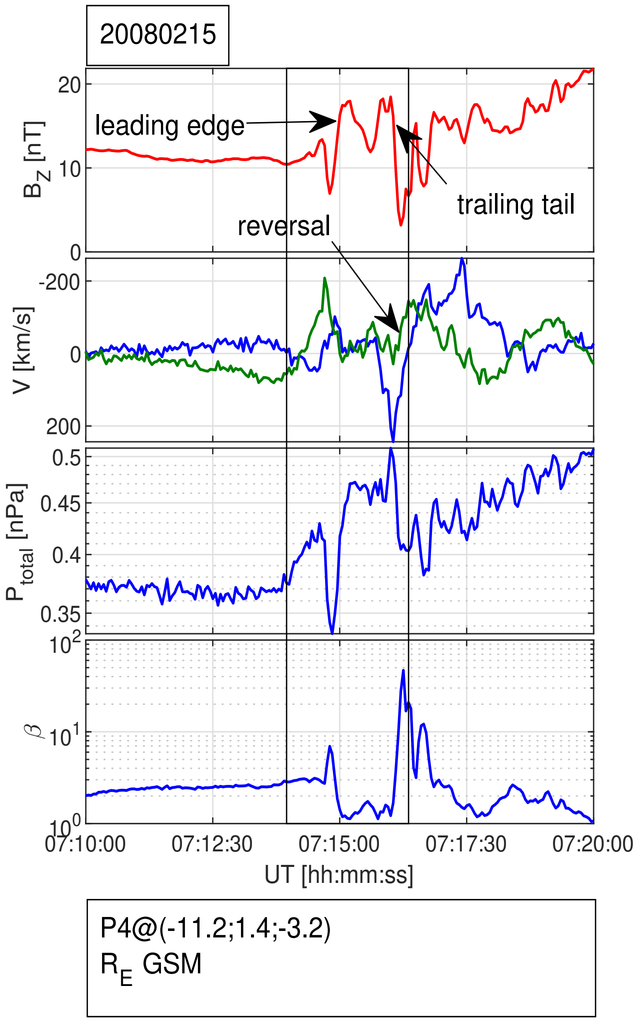

664 **Figure 10.** THEMIS P4 observations during dipolarization front crossing on 15 February 2008 between 7:10 and 7:20 UT. The data are presented in the same layout as each column in Figure 8.

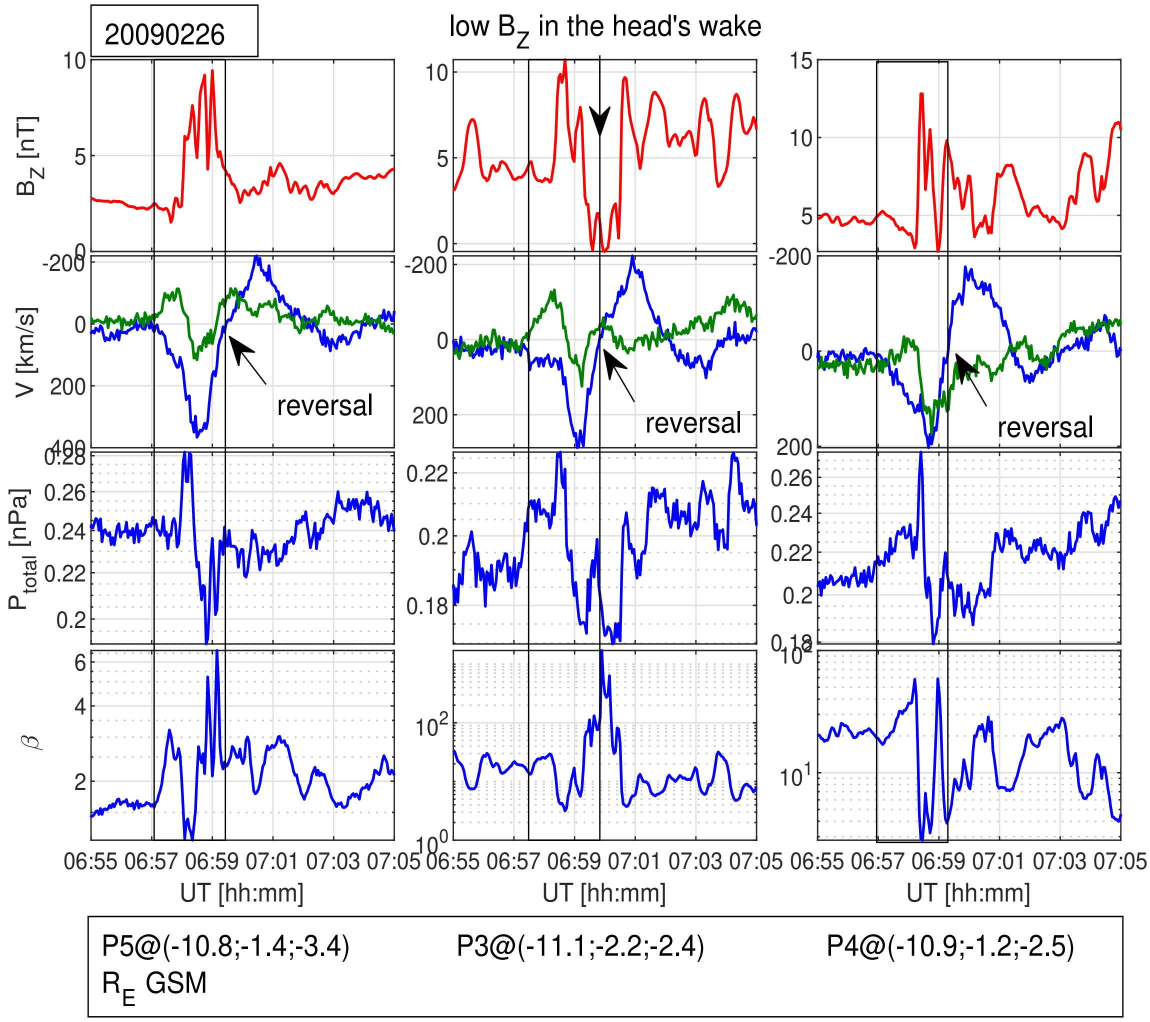

666 **Figure 11.** THEMIS P5 (left), P3 (middle) and P4 (right) observations during dipolarization front crossing
667 on 26 February 2009 between 6:55 and 7:05 UT. The data in each column are presented in the same layout as
668 columns in Figure 8.

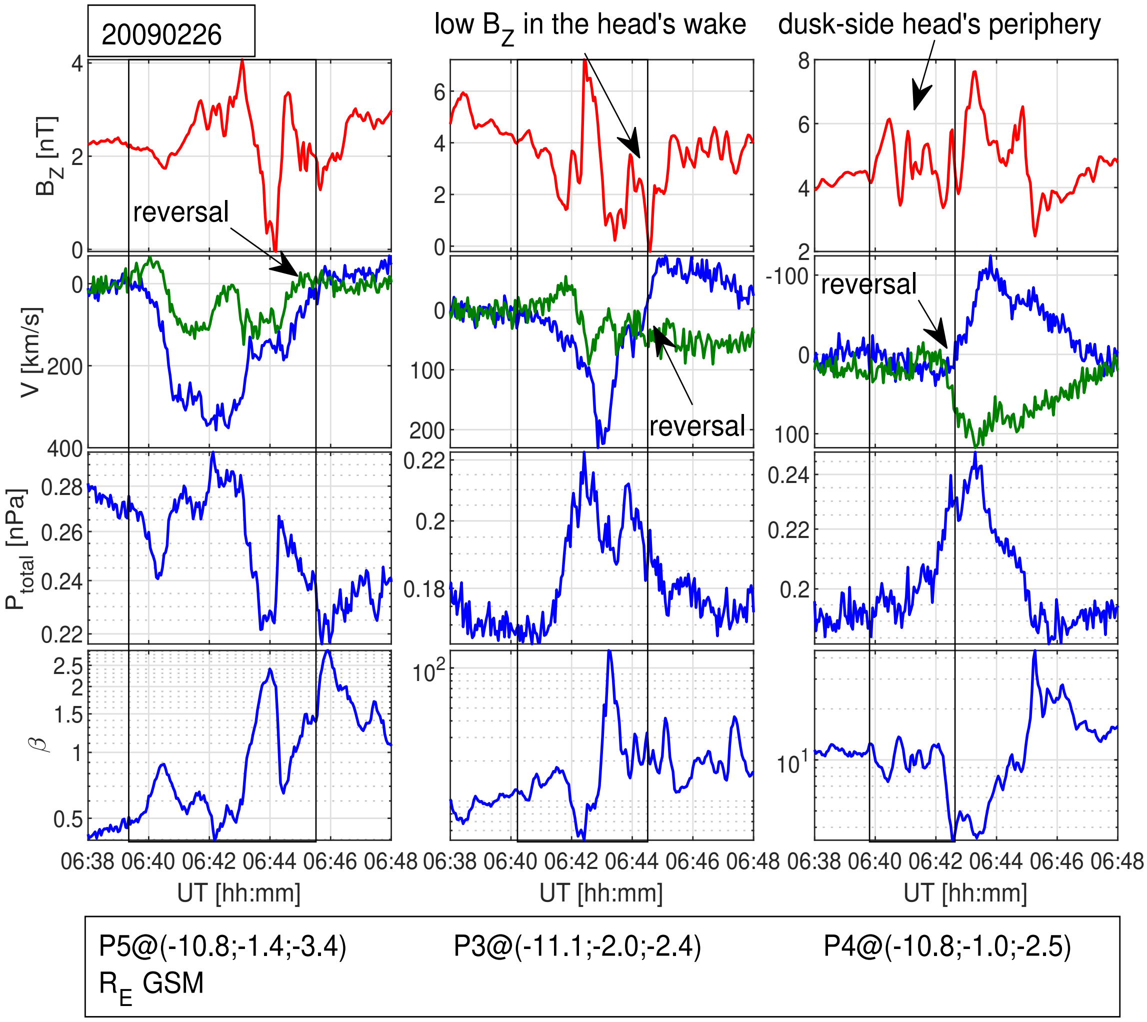

Figure 12. THEMIS P5 (left), P3 (middle) and P4 (right) observations during dipolarization front crossing on 26 February 2009 between 6:55 and 7:05 UT. The data in each column are presented in the same layout as columns in Figure 8.